Synthesis, characterization and low field magnetotransport of $Nd_{0.6}Sr_{0.4}MnO_3/CrO_3$ composite

A. M. Ahmed, H. F. Mohamed, A. K. Diab & Sara A. Mohamed

Indian Journal of Physics

ISSN 0973-1458
Volume 91
Number 2

Indian J Phys (2017) 91:169-181
DOI 10.1007/s12648-016-0908-8

Springer

Indian J Phys (February 2017) 91(2):169–181
DOI 10.1007/s12648-016-0908-8

ORIGINAL PAPER

Synthesis, characterization and low field magnetotransport of $Nd_{0.6}Sr_{0.4}MnO_3/CrO_3$ composite

A M Ahmed*, H F Mohamed, A K Diab and S A Mohamed

Physics Department, Faculty of Science, Sohag University, Sohâg 82524, Egypt

Received: 16 February 2016 / Accepted: 29 June 2016 / Published online: 2 September 2016

Abstract: $(Nd_{0.6}Sr_{0.4}MnO_3)_{1-x}/(CrO_3)_x$ with x = 0.0–0.030 step 0.005 weight% composites have been prepared by the solid state reaction process. The X-ray and scanning electron microscopic manifest that all composites are a single orthorhombic phase and there are no CrO_3 grains separated from NdSrMnO matrix. The electrical measurements have revealed an increase of resistivity and a decrease of metal semiconductor transition with increasing CrO_3. The composite x = 0.025 has largest magnetoresistance nearly one hundred percent at room temperature.

Keywords: Composite material; Electron microscopy; Electrical characterization; Magnetometer; Rietveld analysis

PACS Nos.: 75.47.Lx; 72.80.Tm

1. Introduction

Mixed valence manganites having a stoichiometries form $R_{1-x}A_xMnO_3$ (where R = rare earth element like La, Nd, Pr … and A = alkaline-earth metals like Ca, Sr, Ba), are extensively studied due to their colossal magnetoresistance (CMR) property and also for their rich variety of the physical phenomena [1–5]. The mother compound $LaMnO_3$ is an antiferromagnetic semiconductor (AFS) which develop gradually to a ferromagnetic metal (FMM) when a mixed Mn^{3+}/Mn^{4+} valency is prompted by the R^{3+}/A^{2+} substitution. This is due to the double exchange (DE) interaction between Mn ions, where the carrier spins are aligned and hope from one Mn-site to the other through Mn–O–Mn without change in their spin orientation.

The relative change of the Mn^{3+}/Mn^{4+} ratio is due to different interactions among Mn ions such as double exchange (DE) [5], super-exchange (SE) and coulomb interaction (CI). The competition between these interactions causes a homogeneous and inhomogeneous in electron density distribution. The most pronounced effect of CMR is found in $La_{1-x}Ca_xMnO_3$ films with x = 1/3 [6]. For more than 20 years, researchers and technologists have focused their efforts on the search for new materials with CMR effects and conditions for an increase of CMR effects on the known materials. Spin polarized tunneling studies are well established in granular ferromagnetic (FM)/insulator (I) mixture. Besides, an essential understanding of the CMR mechanism, the intrinsic CMR effect is found on high magnetic field of several Teslas, which restrains its use for practical applications. So there are many efforts to explore materials with low field magnetoresistance (LFMR). It is found that the presence of grain boundaries in polycrystalline manganites cause a large LFMR effect over a wide temperature range. LFMR could be more useful for industrial applications, and it can be attained by different extrinsic properties. One of them is due to the decreasing grain size which is related to spin-dependent scattering and tunneling between neighboring grains [7]. The other is by forming matrix contains these CMR materials with secondary phases. They include LSMO/CeO_2 [8], LCMO/Al_2O_3 [9], LBMO/YSZ [10] and LSMO/ZrO [11]. The basic objective of matrix is to increase the height of the tunnel barrier between neighboring ferromagnetic grains. In this paper, we present the analysis of the magneto-transport and magnetic properties of these matrix system FM –$(Nd_{0.6}Sr_{0.4}MnO_3)_{1-x}$/I–$(CrO_3)_x$.

2. Experimental details

The $(Nd_{0.6}Sr_{0.4}MnO_3)_{1-x}/(CrO_3)_x$ composites with x = 0.0–0.030 wt% step 0.005 were prepared by two steps.

*Corresponding author, E-mail: a.ahmed@science.sohag.edu.eg; fikry_99@yahoo.com

First, the $Nd_{0.6}Sr_{0.4}MnO_3$ powders were prepared in a required ratio by the conventional solid state reaction method. The starting chemical Nd_2O_3, $SrCO_3$ and $MnCO_3$ (high purity powder-99.99 %) were mixed in stoichiometric proportion to prepare the parent compound ($Nd_{0.6}Sr_{0.4}MnO_3$). The mixture was ground for 6 h to ensure homogeneity and presses into pellets under a pressure of 5 ton/cm^2. The pellets were calcined twice for 12 h at 1173 K. Thereafter the pellets were ground, mixed and subsequently sintered in air at 1473 K for 30 h. The obtained $Nd_{0.6}Sr_{0.4}MnO_3$ (NSMO) powders have single-phase perovskite structure. Second, the appropriate weight percentages of the obtained $Nd_{0.6}Sr_{0.4}MnO_3$ (NSMO) and CrO_3 (high purity $\sim$99.99 %) powders were completely mixed and ground. Finally, the mixture was palletized at a pressure of 5 tons/cm^2 and then the sintering was repeated at 1273 K for 6 h. Remarkably, some part of the CrO_3 decomposes to the more stable Cr_2O_3, usually at temperature above 600 °C [12]. The structural characterization was done through X-ray diffraction (XRD) with CuKα radiation at room temperature. The microstructures of samples were studied by Jeol JSM-6610LV scanning electron microscope (SEM). The temperature dependence of resistivity was measured by a standard four point method in zero field and at 0.6 Tesla. The magnetoresistance MR was calculated using the relation $MR = \frac{[\rho(H)-\rho(0)]}{\rho(0)} \times 100\,\%$, where ρ_0 and ρ_H, are the resistivity values for zero and applied fields respectively.

The dc magnetization measurements were done using an EV9 vibrating sample magnetometer (VSM) under applied magnetic field 10 mT. Curie temperature, T_C for each sample has been experimentally defined through the minimum of the first temperature numerical derivative for M (T) curves.

3. Results and discussion

3.1. Structural properties

Figure 1(a) presents the XRD patterns for composites of $(Nd_{0.6}Sr_{0.4}MnO_3)_{1-x}/(CrO_3)_x$. The XRD data analysis clarify that all composites are a single orthorhombic phase with a space group (Pnma). All peaks of the composites satisfy the Nd–Sr–Mn–O phase, and no peaks of impurities or CrO_3 phases could be detected. This may be due to the CrO_3 goes mainly to the perovskite structure $Nd_{0.6}Sr_{0.4}MnO_3$ by reacting and replace Mn^{3+} with Cr^{3+} into it. The same behavior is observed by Kameli et al. [13]. The stander Rietveld refinement technique is utilized for refining the experimental data and calculating the cell parameter of all composites and tabulated in Table 1. Fig. 1(b) depicts the XRD pattern of Cr = 0.010 wt% with its Rietveld refined which affirms no presence of CrO_3.

Noticeable, the peak intensity increases with Cr concentration. This indicates that the CrO_3 and NSMO are coexistent in the composites of NSMO/CrO_3. Furthermore, the angle shift of the diffraction pattern peaks indicates that there is reaction between CrO_3 and NSMO matrix [inset Fig. 1(a)].The lattice parameters and cell volume are changing un-sequentially, also the cell volume for x = 0.015 has largest value as in Table 1. This indicates that some part of CrO_3 goes into the perovskite lattice substituting Mn in NSMO matrix. Because the larger ionic radius of Cr^{+3} (0.615 Å) with Mn^{+3} (0.58 Å) [14], the lattice parameters expand.

The XRD results allow to calculate the average crystallite size of the materials using Scherer's formula, $CS = k\lambda/\beta \cos(\theta)$, where k is a constant (shape factor of 0.89), λ is the CuKα wavelength, and β is the full width half maximum (FWHM) of XRD peak. The crystallite sizes are found to be in the range 14.79–20.5 nm.

The typical SEM micrographs and analysis of Energy-dispersive X-ray spectroscopy for the composites are shown in Figs. 2(a)–2(h). The results of the compositions are summarized in Table 2. No trace of any impurity is found, indicating the purity of the composite. Also, there is no loss any ingredient after preparation process. The EDAX data suggest that the predecessors have fully suffered the chemical reaction to form the expected perovskite composite. Moreover, the percentage of Cr is un-sequentially (as EDAX Table 2) and the composite of x = 0.015 has large value of CrO_3 that confirms its cell volume is larger. The reason for EDAX characterization is to ratify the purity and surety of the chemical composition but it is not accurate to determine the ratio content of elements especially the oxygen content which is light element.

Regarding the SEM images, it is found that the clear grain boundary is observed in all composites and no any trace of CrO_3. This means that the CrO_3 goes into the perovskite lattice and probably a little part of the Cr_2O_3 is in the grain boundaries. This amount in grain boundary is low, so it is difficult to appear in the SEM image. Obviously, the grain sizes observed by SEM (Table 1) are in μm range where the CS estimated by XRD is in nm range, which indicates that each grain observed by SEM consists of several crystallites.

3.2. Magneto-transport properties

Figure 3 shows the electrical resistivity versus temperature ρ(T) plots, measured in zero field for $(Nd_{0.6}Sr_{0.4}MnO_3)_{1-x}/(CrO_3)_x$. It is found that the resistivity increases systemic as the chromium increase except the composite x = 0.015

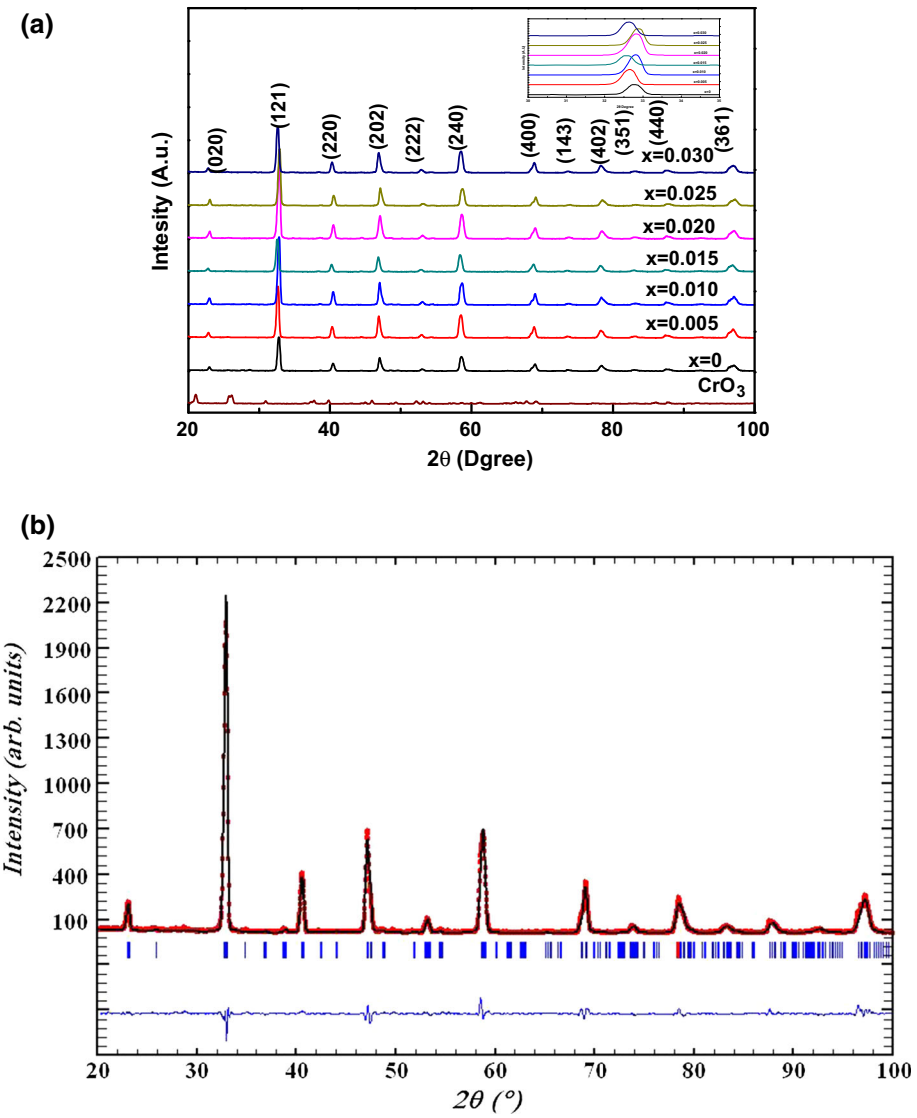

Fig. 1 (**a**) X-ray diffraction patterns of $(Nd_{0.6}Sr_{0.4}MnO_3)_{1-x}(CrO_3)_x$ (0.0–0.030 step 0.005 wt%), the *inset* shows the variation of peak shape with doping for 121 peak. (**b**) Rietveld plot of XRD pattern of $(Nd_{0.6}Sr_{0.4}MnO_3)_{0.99}(CrO_3)_{0.\ 010}$, *black dots line* indicates the experimental data, the *line* overlapping them indicates calculated profiles. The lowest *curve* shows the difference between experimental and calculated patterns. The *vertical bars* are the expected Bragg's positions

Table 1 Crystal lattice parameters, the cell volume, the average grain size (μm) and crystal size (nm) of $(Nd_{0.6}Sr_{0.4}MnO_3)_{1-x}/(CrO_3)_x$

Sample	a (Å)	b (Å)	c (Å)	V ($Å^3$)	Crystal size (nm)	Average grain size (μm)
0	5.464	7.710226	5.40859	227.8567	14.79	0.33
0.005	5.486	7.716808	5.425292	229.6765	16.39	0.49
0.010	5.462	7.711632	5.408586	227.8147	20.5	0.56
0.015	5.498	7.723084	5.420731	230.1725	16.39	0.49
0.020	5.458	7.707111	5.418748	227.9419	15.18	0.52
0.025	5.45	7.70541	5.413172	227.3234	20	0.78
0.030	5.49	7.714029	5.409612	229.0972	16.39	0.60

and 0.020 wt%. The composites for $x \leq 0.025$ wt% exhibit transition from semiconducting state $(\frac{d\rho}{dT} < 0)$ to a metallic one $(\frac{d\rho}{dT} > 0)$ at a certain temperature (T_{ms}), in contrast for $x = 0.030$ wt% there is no metal–semiconductor transition.

The transition temperature value (T_{ms}) decreases with the increasing of the CrO_3 content. The observed change of T_{ms} and ρ with increasing the doping can be interpreted as CrO_3 goes inside the grains by replacing Mn site in the NSMO matrix. This cannot contribute in the double

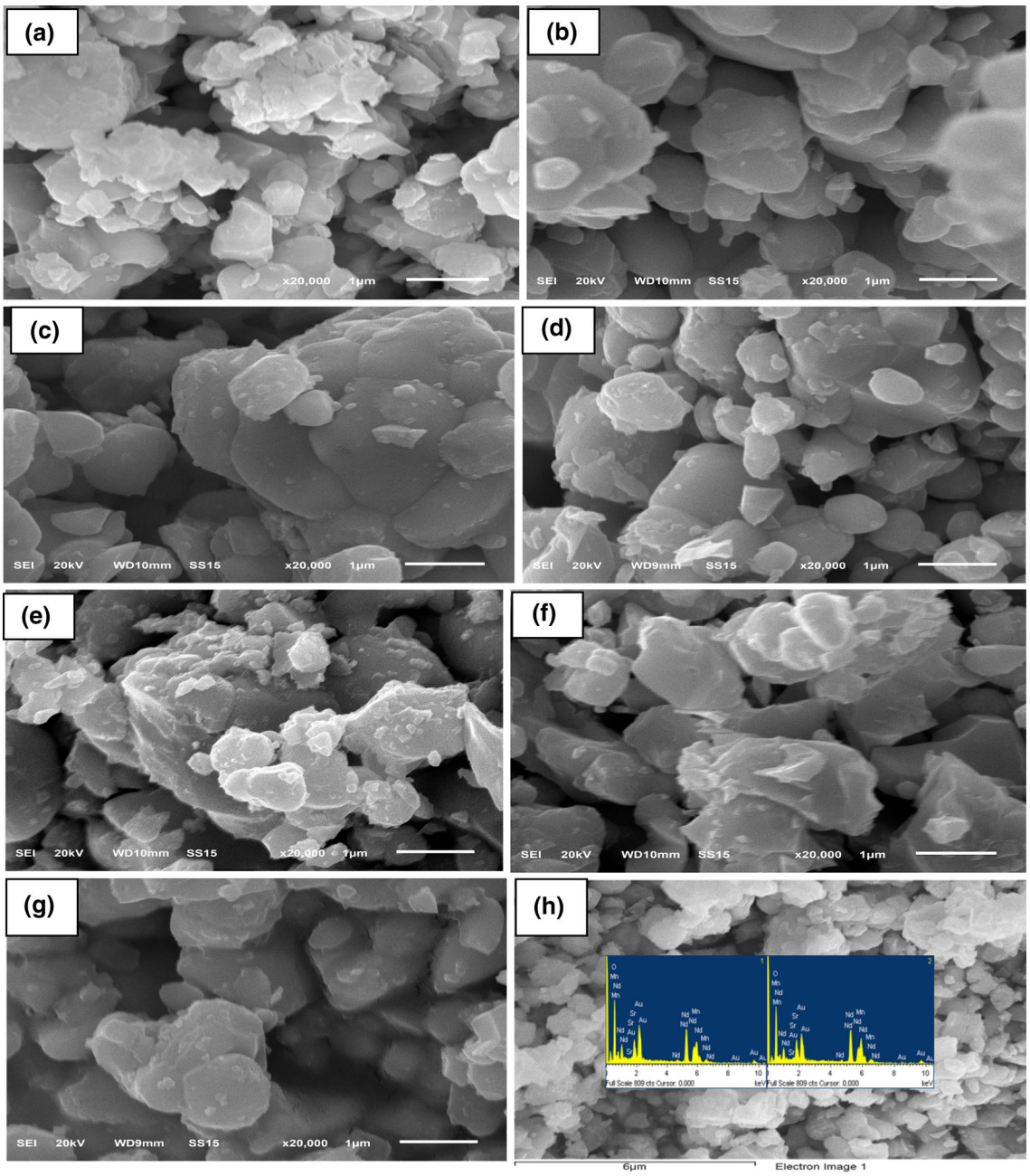

Fig. 2 SEM of $(Nd_{0.6}Sr_{0.4}MnO_3)_{1-x}/(CrO_3)_x$ composites (**a**) x = 0, (**b**) x = 0.005, (**c**) x = 0.010, (**d**) x = 0.015, (**e**) x = 0.020, (**f**) x = 0.025, (**g**) x = 0.030 and (**h**) x = 0 for EDAX

Table 2 The percentage contents of elements as EDAX chart

Sample	Cr %	O %	Mn %	Sr %	Nd %
0	0	39.87	11.73	9.37	39.03
0.005	1.62	35.48	19.42	13.66	29.82
0.010	0.7	35.11	19.59	14.34	30.26
0.015	1.78	31.36	21.62	12.35	32.88
0.020	0.64	27.38	23.55	13.19	35.24
0.025	1.66	26.74	23.83	12.60	35.17
0.030	1.62	35.48	19.42	13.66	29.82

exchange (DE) mechanism involving Mn^{3+} and Mn^{4+} ions, so it dilutes the DE process.

Concerning, the composite x = 0.015, observed that its resistivity is smaller than the others, conversely the percentage of Cr (as EDAX Table 2). This may be due to the most part of Cr_2O_3 has occupied interstitial sites on the grain boundaries [15], which lead to decreases the resistivity, and the remainder goes to inside the grain and grain boundaries.

Besides, there is rapidly increasing in the resistivity of composite x = 0.020 with lower percentage of Cr (as

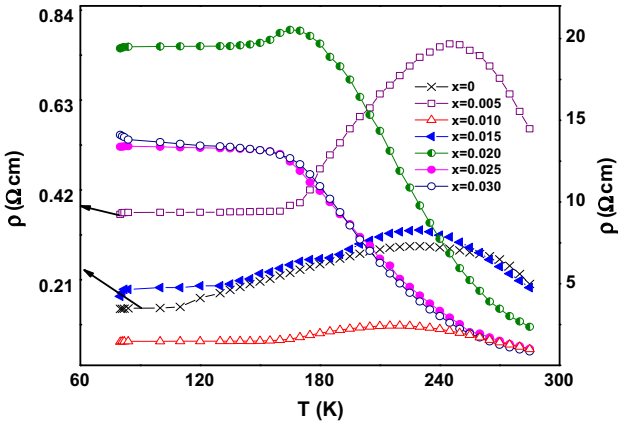

Fig. 3 The temperature dependence of the resistivity for $(Nd_{0.6}Sr_{0.4}MnO_3)_{1-x}/(CrO_3)_x$ in absent magnetic field

EDAX Table 2). This suggests that there are two conduction channels parallel connected in this composite. One is related to grains and the other is related to grain boundary. Accordingly, in this composite some of CrO_3 or Cr_2O_3 goes inside the grains and the residual goes inside grain boundaries [15].

Figure 4 presents the effect of applied Low magnetic field (0.6 T) on the resistivity for all composites. As shown in the figure, the applying magnetic field decreases the resistivity throughout the temperature range and T_{ms} shifts slightly to a higher temperature [16, 17]. This shift is owing to alignment of the Mn spins that causes the suppression of the semiconducting state by metallic state. Because of the spin ordering, the charge carries also suffer less scattering with the increase of the exchange interaction, hence the resistivity decreases, and a large negative magnetoresistance (MR) occurs.

It is seen that the effect of magnetic field on the resistivity is much more in low temperature for the composites $x \geq 0.015$ wt%. This due to spin ordering is more pronounced in this range.

In order to analyze the temperature dependence of *MR* % plots depicted in Fig. 5, there are two different mechanisms described the appeared maximum magnetoresistance should be taken in consideration. The first one is the intrinsic magnetoresistance (*i-MR*) which arises due to the suppression of spin fluctuations by aligning the spins due to applying a magnetic field. It is notable that the maximum of the *i-MR* near the ferromagnetic transition temperature. The second one is the extrinsic magnetoresistance (*e-MR*) which arises due to inter-grain spin polarized tunneling across the insulating boundaries or spin polarized scattering, which occurs at the grain boundaries with magnetic inhomogeneity [11, 18–20].

The *e-MR* of the composites $x \leq 0.020$ is due to spin polarized scattering (except composite $x = 0.015$). This is agreement with the suggestion of Liu et al. [21]. The suggestion is the spin polarized scattering may have been dominant than spin polarized tunneling for low temperature *MR*. Spin-dependent scattering may arise from the decomposition of some CrO_3 into the more stable Cr_2O_3, which is an antiferromagnetic insulator and may serve as the scattering centers [11]. Otherwise, for the composite $x = 0.015$ the spin polarized tunneling is dominant than spin polarized scattering causes some part of Cr_2O_3 has occupied interstitial sites on the grain boundaries which it acts spin tunneling.

Furthermore, appearance of the two maxima (*i-MR* and *e-MR*) in the *MR*-T plots (see Fig. 5), confirms that both mechanisms are strongly effective in the present case. Finally, the composite $x = 0.025$ has largest magnetoresistance nearly one hundred percent at room temperature. This is a large edifice in the magnetoresistance material, so the authors command strongly to apply this composite in industrial applications.

3.3. Conduction mechanisms

At temperature lower than transition temperature (characterized by FM phase) of the ρ–T plots measured with and without magnetic field is found to be well represented by the empirical relation (as seen in Fig. 4)

$$\rho = \rho_0 + \rho_2 T^2 + \rho_{4.5} T^{4.5} \quad (1)$$

where the terms ρ_0, $\rho_2 T^2$ and $\rho_{4.5} T^{4.5}$ are arise due to the grain/domain boundary [22, 23], the electron–electron scattering [24] and the electron-magnon scattering process [25] respectively.

As shown in Table 3, the fitting parameters continuously increase with increasing the dopant amount (except $x = 0.015$). The domains become large, thereby reducing the value of ρ_0. In fact the increment of ρ_2 and $\rho_{4.5}$ with the doping is due to the suppression of spin fluctuation. Hence, the bandwidth becomes smaller that causes weakening the DE (confirms the earlier interpretation). On the other hand the alignment of the spins, in the applied magnetic field suppresses various scattering contributions and as a result ρ_0, ρ_2 and $\rho_{4.5}$ decreases with applying the magnetic field.

At temperature higher than transition temperature (characterized by the semiconducting phase) can be divided into two distinct parts described by two different mechanisms. The first one lies in the range $T_{ms} \leq T \leq \Theta_{D/2}$ (Θ_D is the Debye's temperature) and is well described by the variable range hopping (VRH) model proposed by Mott and

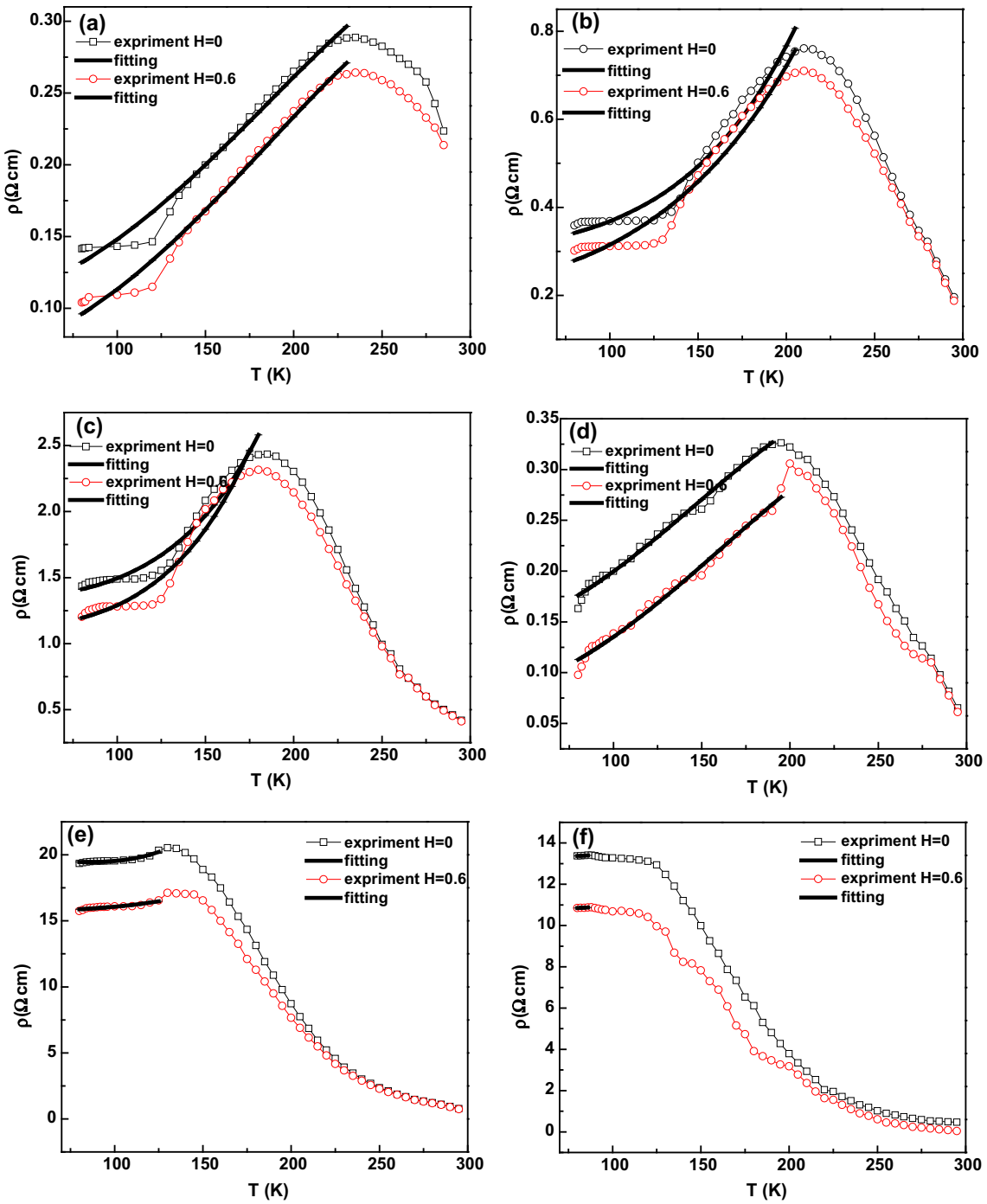

Fig. 4 The resistivity versus temperature for H = 0 and H = 0.6 T of $(Nd_{0.6}Sr_{0.4}MnO_3)_{1-x}/(CrO_3)_x$, (**a**) x = 0, (**b**) x = 0.005, (**c**) x = 0.010, (**d**) x = 0.015, (**e**) x = 0.020, (**f**) x = 0.025 and (**g**) x = 0.030. The *black line* represents the best fit to the Eq. (1)

Davis [26]. The half of the value of Θ_D is defined as the temperature at which deviation from linearity in ln(σ) versus $T^{-1/4}$ plots occurs. The second part (at $T \geq \Theta_{D/2}$) fits well with the small polaron hopping (SPH) model.

According to the VRH mechanism the temperature dependence of resistivity is represented by the equation,

$$\sigma = \sigma_\circ \exp\left(\frac{T_\circ}{T}\right)^{\frac{-1}{4}} \tag{2}$$

where σ_0 is a pre-exponential factor, T_0 is a constant [= 16 $\alpha^3/k_B N(E_f)$] and $N(E_f)$ $\left[= 16\frac{\alpha^3}{k_B N(E_f)}\right]$ and $N(E_f)$ is the

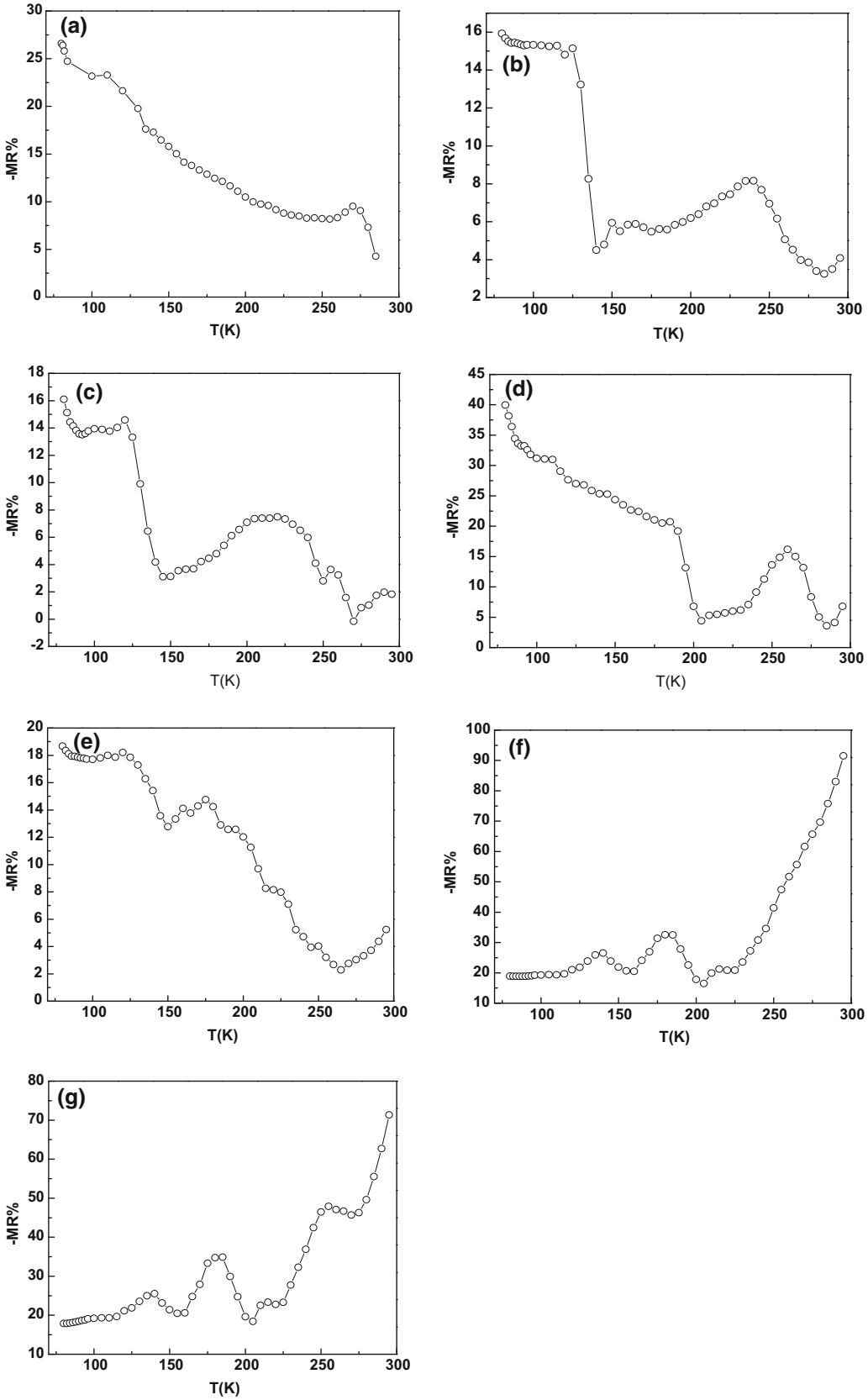

Fig. 5 The temperature dependence of magnetoresistance of $(Nd_{0.6}Sr_{0.4}MnO_3)_{1-x}/(CrO_3)_x$ (**a**) x = 0, (**b**) x = 0.005, (**c**) x = 0.010, (**d**) x = 0.015, (**e**) x = 0.020, (**f**) x = 0.025 and (**g**) x = 0.030 under magnetic field = 0.6 T

Table 3 The best-fit parameters at low temperature ($T < T_{ms}$) resistivity data in magnetic field = 0.0 and 0.6 T for $(Nd_{0.6}Sr_{0.4}MnO_3)_{1-x}/(CrO_3)_x$

Sample	ρ_0 (Ω cm)		ρ_2*10^{-5} (Ω cm/K^2)		$\rho_{4.5}*10^{-11}$ (Ω cm/K$^{4.5}$)	
	H = 0 T	H = 0.6 T	H = 0 T	H = 0.6 T	H = 0 T	H = 0.6 T
0	0.1025	0.0646	0.46	0.498	−0.126	−0.135
0.005	0.3028	0.221	0.54	0.869	1.08	0.67
0.010	1.31	1.08	1.22	1.26	6.22	8
0.015	0.132	7.09	0.711	0.669	−0.346	−0.26
0.020	19.91	15.6	−11.4	3.34	76.7	12.1
0.025	–	–	–	–	–	–
0.030	–	–	–	–	–	–

density of states at Fermi level which is calculated from the slope of the $\ln\sigma$ vs . $T^{-1/4}$ curves (as shown Fig. 6). The hopping distance (R) and hopping energy (W) can be written, at a given temperature T, as

$$R = \left[\frac{9}{8\pi\alpha k_B T N(E_f)}\right]^{1/4} \tag{3}$$

$$W = \left[\frac{3}{4\pi R^3 N(E_f)}\right] \tag{4}$$

The values of $N(E_f)$ R and W at room temperature are estimated by taking $\alpha = 2.22\ nm^{-1}$ [24] and have been listed in Table 4. Obviously, the calculated values are very close to those reported in other works [23, 27, 28].

Also, the dopant has significant effect on the calculated parameters where the T_0 increases up to x = 0.020 and decreases thereafter while $N(E_f)$ shows opposite trend. The increase of the T_0 value is argued to weaken the DE.

Furthermore, T_0 values are found to be smaller in the presence on the field and as a result, the density of states at Fermi level increases. This can be due to the suppression of the magnetic domain scattering with application of the magnetic field [29], υ_{ph} (the optical phonon frequencies) is determined from the relation $h\upsilon_{ph} = k_B\theta_D$. It seems that $\theta_D/2$ is higher than T_{ms} (Table 4), which reveal that the VRH mechanism dominate over a wide range of the temperature of measurements. In general, increment CrO_3 leads to a decrease in T_{ms}. Since the interaction of Mn^{3+}–Mn^{4+} is ferromagnetic one, the transition to a ferromagnetic state enables electron hops between Mn^{3+} and Mn^{4+} ions without spin flip, and so the hopping resistance falls. Reducing the temperature and the application of an external magnetic field makes spin reverse even more difficult and this leads to a further decrease in resistance which result in MR.

As mentioned above, at $T \geq \theta_D/2$, the conduction mechanism is described by the thermally activated hopping of small polarons [30] and fits well with the SPH model [26].

$$\frac{\rho}{T} = \rho_\alpha \exp\left(E_\rho/k_B T\right), \tag{5}$$

where ρ_α is the resistivity coefficient, E_ρ is the activation energy and k_B is the Boltzmann constant. The activation energy E_ρ is determined from the slope of the $\ln\left(\frac{\rho}{T}\right)$vs.$\frac{1}{T}$ plots presented in Fig. 7.

As shown in Table 4, after initial sample, E_ρ decreases by CrO_3 doping up to 0.015. However, it exhibits also decrease in the high doping except x = 0.025 Such decrease is interpreted by considering that increasing CrO_3 doping level causes charge delocalization (due to the decrease of γ or electron–phonon interaction constant) and thereby the energy required to liberate a free carrier is decreased.

The activation energies estimated from ρ(T) variation in the present or absent magnetic field and observed that under magnetic field, the activation energy decreases for every doping concentration (Table 4). This is due to delocalization of charge carriers reported earlier and spin ordering in the system [31]. For polaron hopping conduction [26].

$$E_\rho = W_H + W_D/2 \left(\text{for } T > \frac{\theta_D}{2}\right) \text{and } E_\rho = W_D \text{ for } T < \theta_D/4 \tag{6}$$

where W_H is the polaron hopping energy and W_D is the disorder energy.

In order to present a complete comprehensive study on the conduction mechanism of the materials, we try to find out the nature of the hopping conduction (adiabatic or non-adiabatic). It is recognized from Holstien's relation [32] that the polaron bandwidth realize the conditions $J > H$ or $J < H$ for adiabatic or non-adiabatic hopping conduction respectively. Where

$$H = (2k_B T W_H/\pi)^{1/4}(h\upsilon_{Ph}/\pi)^{1/2} \tag{7}$$

The condition should be realized for the small polaron formation is $J \leq \frac{W_H}{3}$ [32], J can be evaluated from the approximate relation for the high temperature jump site

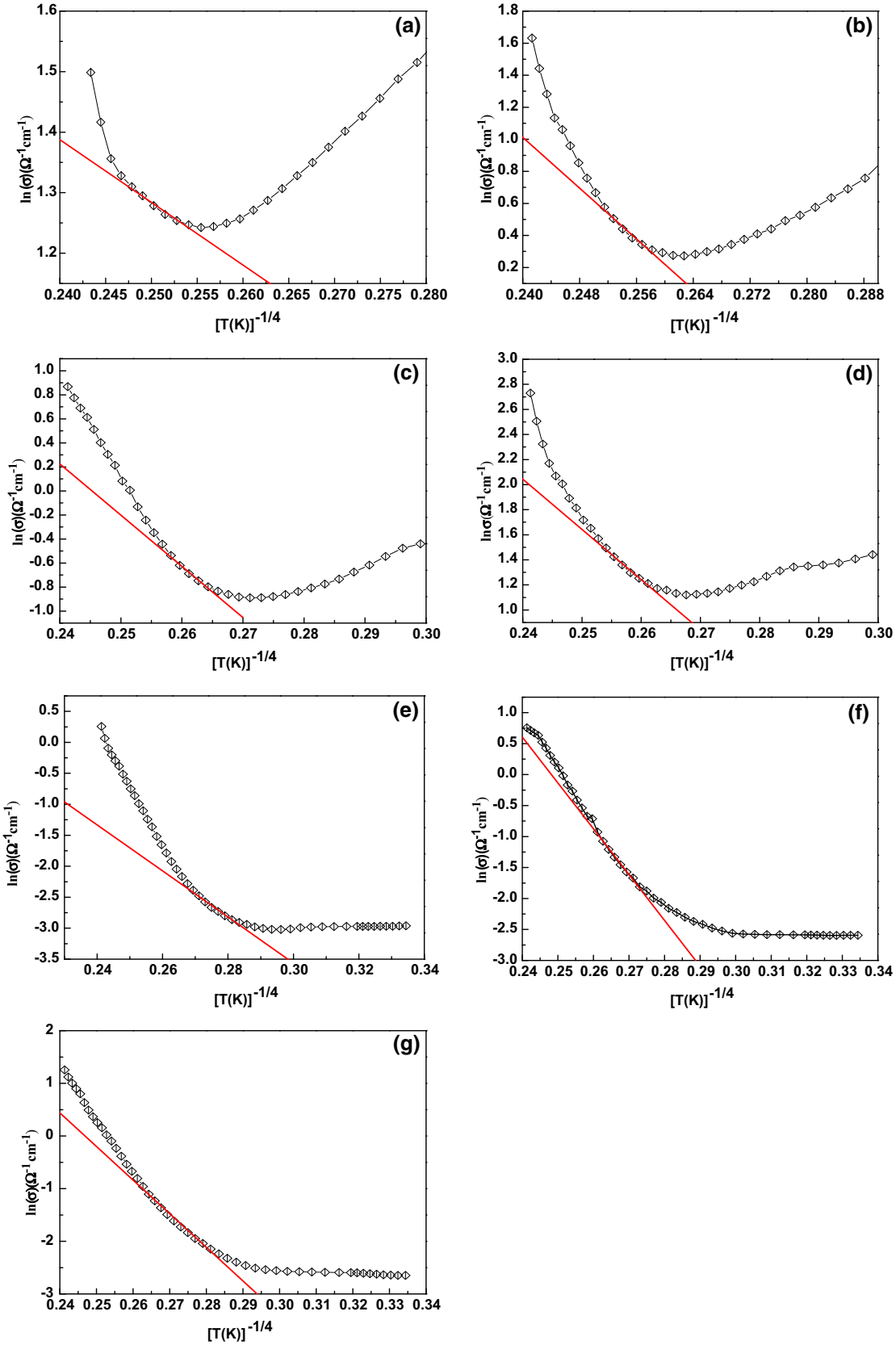

Fig. 6 ln(σ) versus $T^{-1/4}$ of $(Nd_{0.6}Sr_{0.4}MnO_3)_{1-x}/(CrO_3)_x$ composites without magnetic field, where (**a**) x = 0, (**b**) = 0.005, (**c**) x = 0.010, (**d**) x = 0.015, (**e**) x = 0.020, (**f**) x = 0.025 and (**g**) x = 0.030. The *red line* represents the best fit to the Eq. (2) (color figure online)

Table 4 T_{ms} (K), T_C (K), E_{ρ} **(Ev)**, E_{ρ} (mev), θ_D (K), υ_{ph} (Hz), $W_{H\rho}$ (mev), γ_{Ph} and exp (γ_{Ph}) of $(Nd_{0.6}Sr_{0.4}MnO_3)_{1-x}/(CrO_3)_x$ with and without magnetic field

Sample	X = 0 wt%		X = 0.005 wt%		X = 0.010 wt%		X = 0.015 wt%		X = 0.020 wt%		X = 0.025 wt%		X = 0.030 wt%	
	H = 0 T	H = 0.6 T	H = 0 T	H = 0.6 T	H = 0 T	H = 0.6 T	H = 0 T	H = 0.6 T	H = 0 T	H = 0.6 T	H = 0 T	H = 0.6 T	H = 0 T	H = 0.6 T
T_{ms} (K)	235	235	210	210	185	180	195	200	135	130	88	88	–	–
T_C (K)		273		294		287		273		279		289		286
θ_D (K)	540.5	509.4	500	520.8	459.8	510.2	459.8	540.5	510.2	540.5	400	500	439.6	530.5
ν_{ph} (Hz) $\times 10^{12}$	11.3	10.6	10.4	10.9	9.5	10.6	9.6	11.3	10.6	11.3	8.3	10.4	9.2	11.1
$\rho_0 \times 10^{-6}$	2.9	57.7	1.1	0.37	4.45	3.1	1.04	0.001	0.57	0.008	5.98	–	5.7	–
E_{ρ} (meV)	137.5	63.4	165.1	91.4	146.8	65.2	141.9	56.4	215.4	130.1	140.4	44.8	138.3	34.2
W_H (meV)	119.4	–	150.1	–	119.2	–	111.7	–	203.6	–	123.7	–	120	–
WH/3 (meV)	39.7	–	50.02	–	39.7	–	37.2	–	67.9	–	41.2	–	54.9	–
WD (meV)	238.7	–	300.1	–	238.5	–	223.3	–	407.2	–	247.3	–	226.8	–
H (meV)	25.4	–	25.9	–	23.4	–	23.05	–	28.2	–	22.1	–	21.8	–
J (meV)	25.2	–	25.7	–	23.2	–	22.9	–	25.6	–	21.3	–	21.3	–
γp	5.1	–	6.9	–	6.02	–	5.3	–	9.3	–	7.2	–	6.7	–
Exp (γp)	168.1	–	1060.01	–	411.38	–	280.6	–	10,538.1	–	1308.9	–	812.4	–
T_0 (K) $\times 10^6$	1.5	1.003	0.9	0.82	1.4	1.05	1.4	1.12	7.8	5.8	10.03	9.2	3.4	2.5
N (EF)(eV-1 cm^{-3}) $\times 10^{20}$	13.5	15.5	22.5	13.5	14.9	0.26	14.7	0.65	12.3	0.35	13.5	0.33	0.59	10.04
N $\times 10^{23}$	24.5	13.4	41.04	24.6	27.1	0.47	26.8	1.18	0.47	0.64	3.7	0.59	1.1	0.08
R (À) $\times 10^{-7}$	1.5	0.3	1.3	1.5	1.4	3.9	1.4	3.1	3.9	3.6	2.4	3.7	3.2	6.2
W (meV)	54.7	11.3	48.1	54.7	53.4	147.1	53.5	116.8	147.08	136.2	147.1	138.4	119.5	229.7
αR	3.3	0.68	2.9	3.3	3.2	8.8	3.2	7.01	8.8	8.1	8.8	8.3	7.2	13.8

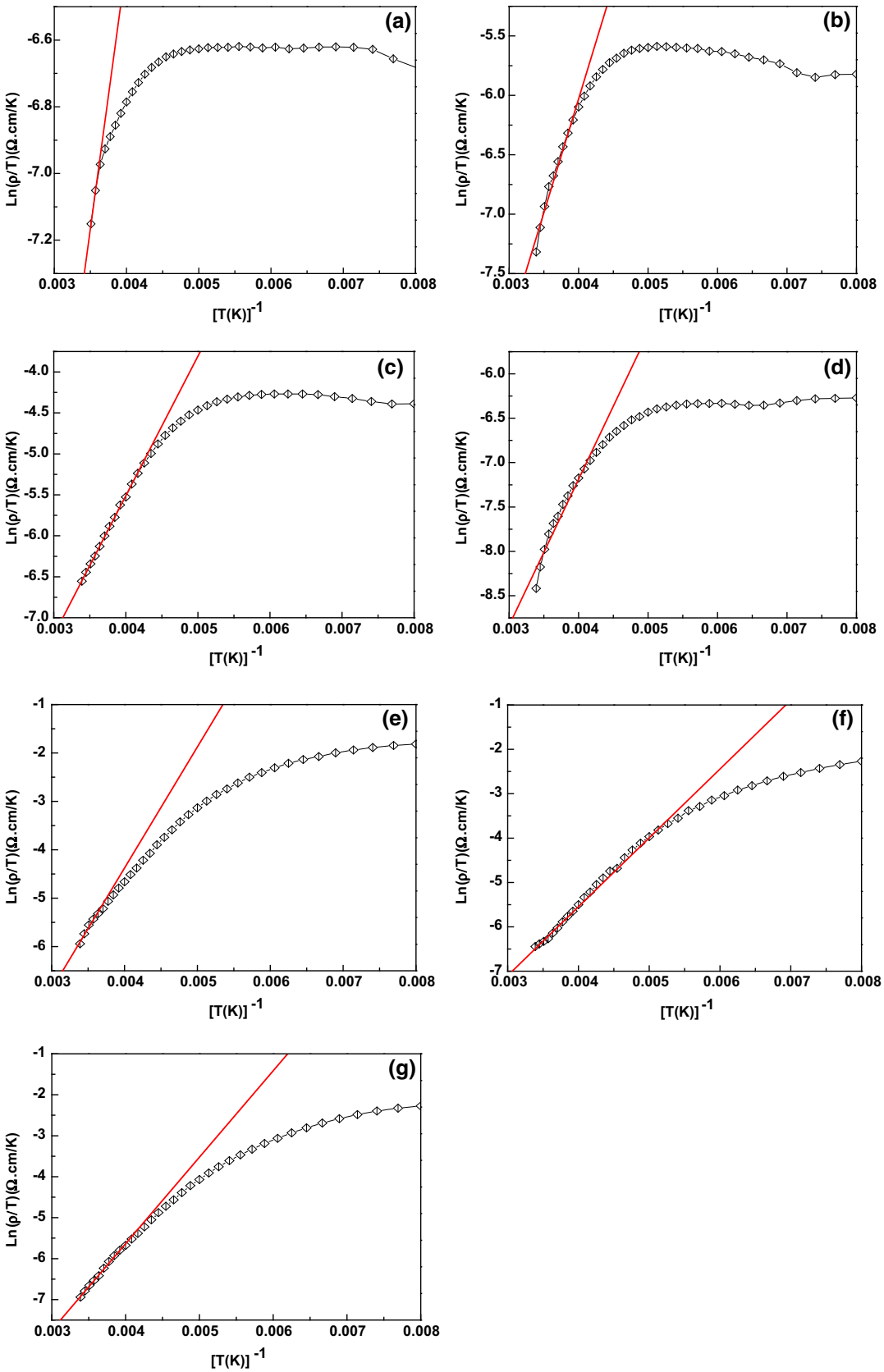

Fig. 7 Variation of ln(ρ/T) versus 1/T of $(Nd_{0.6}Sr_{0.4}MnO_3)_{1-x}/(CrO_3)_x$ composites without magnetic field, where (**a**) x = 0, (**b**) x = 0.005, (**c**) x = 0.010, (**d**) x = 0.015, (**e**) x = 0.020, (**f**) x = 0.025 and (**g**) x = 0.030. The *red line* represents best fit to the Eq. (5) (color figure online)

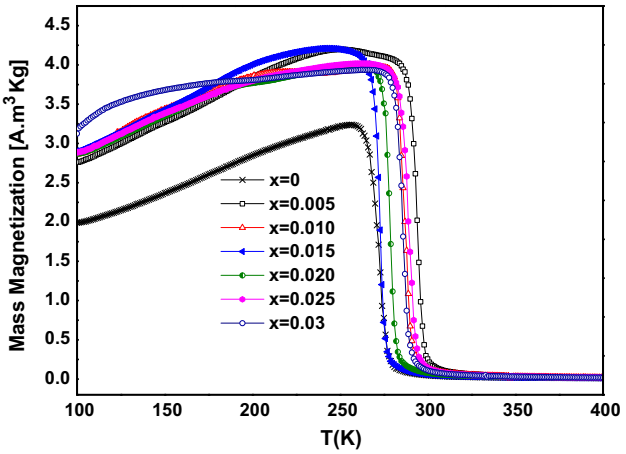

Fig. 8 The temperature dependence of mass magnetization of $(Nd_{0.6}Sr_{0.4}MnO_3)_{1-x}/(CrO_3)_x$ composites

$$J(T) \approx 0.67 h\nu_{ph}(T/\theta_D)^{1/4} \quad (8)$$

The data presented in Table 4 show that J (290 K) < H and J (290 K) < $W_H/3$, which confirm that the DC conduction in the system due to SPH as non-adiabatic regime. We have used the relation $\gamma_{Ph} = \frac{2W_H}{h\nu_{Ph}}$ [29] to estimate the small polaron coupling constant (γ), which is a measure of the electron–phonon interaction constant of the sample. It is found that γ decreases as the CrO_3 content increases (see Table 4).

3.4. Magnetization

The temperature dependence of magnetization is studied in zero field M $(T)_{ZFC}$ cooling regimes at a fixed applied magnetic field 10 mT within a temperature rang 100–450 K. For composites $x \leq 0.015$ the T_C values decrease as the doping increase and then increase with further CrO_3 content for $x = 0.020$ and 0.025. This decrease is due to magnetic dilution which comes from the substitution of the Cr^{3+} ion for Mn^{3+} ion weakens the DE [33]. Fig. 8 illustrates that the M $(T)_{ZFC}$ of all the composites except for $x = 0.03$ shows a drop in the magnetic moment, indicating the ferromagnetic order is weakened and magnetic disorder is increased with the Cr content. Thus, inclusion of antiferromagnetic Cr_2O_3 dilutes the magnetization of composites. However, the gradual decrease in magnetic moment for $x = 0.030$ below T_C is due to the short range ordering short-range FM ordering.

4. Conclusions

We have presented a detailed set of structural, magneto-transport, and magnetization measurements on composites of $(Nd_{0.6}Sr_{0.4}MnO_3)_{1-}(CrO_3)_x$ with $x = 0.0$–0.030 step 0.005. In magnetic properties, all composites undergo a sharp FM to PM transition.

In magneto-transport properties, we observe the composites for $x \leq 0.020$ wt% exhibit transition from semiconducting state to a metallic one with lowering temperature. Beside for $x \geq 0.025$ wt% there is no metal semiconductor transition. The composite for $x \leq 0.020$ wt%, magnetoresistance contribution increases as the temperature decreases while on contrary for $x \geq 0.025$ wt%.

The SPH mechanism might be suitable to explain the electrical resistivity in the high temperature. The composite $x = 0.025$ has largest magnetoresistance nearly one hundred percentage at room temperature. This is a large edifice in the magnetoresistance material.

References

[1] R yon Helmot, J Wecker, B Holzapfel, L Schultz and K Samwer, *Phys. Rev. Lett*. **71** 2331 (1993)
[2] G H Jonker and J H van Santen, *Physica (Utrecht)* **16** 337 (1950)
[3] J E O Wollan and W C Koehler, *Phys. Rev*. **100** 545 (1955)
[4] C Zener, *Phys. Rev. B*. **82** 403 (1951)
[5] C Zener, *Phys. Rev*. **181** 440 (1951)
[6] B I Belevtsev et al, *phys. stat. sol. (a)* **188 No. 3** 1187 (2001)
[7] S Jin, T H Tiefel, M Mc Cormack, R A Fastnacht, R Ramesh and L H Chen, *Science* **264** 413 (1994)
[8] Y Okimoto, Y Tomioka, Y Onose, Y Otsuka, and Y Tokura, *Phys. Rev. B* **57** R9377 (1998)
[9] J B Goodenough and J-S Zhou, *Nature(London)***386** 229 (1997)
[10] T Terai et al., *Phys. Rev. B* **58** 14908 (1998)
[11] H Hwang, S W Cheong, NP Ong and B Batlogg, *Phys Rev Lett***. 77** 2041 (1996).
[12] C B Stagarescu et al., *Phys. Rev. B* **61** R9233 (2000)
[13] P Kameli, H Salamati, M Eshraghi, and M R Mohammadizadeh, *J. Appl. Phys.* **98** 043908 (2005)
[14] R D Shannon, *Acta Crystallogr A* **32** 751(1976)
[15] A M Ahmed, H F Mohamed, A K Diab, Abd El-Mo'ez A Mohamed, A E A Mazen and A M Mohamed, *Indian J Phys,* **89(6)** 561 (2015)
[16] A M Ahmed, G Papavassiliou, H F Mohamed and E M M Ibrahim, *J. Magn. Magn. Mat*. **392** 27 (2015)
[17] A M Ahmed, A K Diab and H F Mohamed, *J. Supercond Nov Magn.* **24** 597 (2011)
[18] X W Li, A Gupta, G Xiao and G Q Gong, *Appl. Phys. Lett.* **71** 1124 (1997)
[19] A M Haghiri-Gosnet and J P Renard,*J. Phys. D:Appl. Phys*. **36** 127 (2003)
[20] A Gupta et al. *Phys. Rev. B* **54** 15629 (1996)
[21] S J Liu, J Y Juang, K H Wu, T M Uen, and Y S Gou, *Chin. J. Phys.* **41** 406 (2003)
[22] K Gunnarson, P Svedlindh, P Nordblad, L Lundgren, H Aruga and A Ito, *Phys. Rev. Lett*. **61** 754(1988)
[23] G Venkataiah et al., *Physica B* **357** 370 (2005)
[24] M Viret, L Ranno and J M D Coey*Phys. Rev. B* **55** 8067 (1997)
[25] G J Snyder, R Hiskers, S DiCarolis, M R Beasley, T H Geballe, *Phys. Rev. B* **53** 14434 (1996)
[26] N F Mott and E A Davis *Electronics Process in NonCrystalline Materials,* 2nd edn. (Oxford: Clarendon press) (2012)

[27] K M Satyalakshmi, B Fisher, L Patlagan, and G Koren, *App. Physc. Lett.* **73** 320(1998)
[28] N El- S F Hamad PHD in physics "Magnetic and Electrical Properties of $Nd_{0.66}$ $(Sr_{1-y}Li_y)_{0.34}MnO_3$manganites" Institute of physics Gerog-August University, Goettingn, Germany December (2003)
[29] N F Mott and I G Austin, *Adv. Phys*. **18** 41 (1969)
[30] G H Rao, J R Sun, K Bärner and N Hamad, *J. Phys.: Condense. Matter* **11** 1523 (1999)
[31] S Battacharya, S Pal, A Banerjee, H D Yang and B K Chaudhuri, *J. Chem. Phys.* **119** 3972 (2003)
[32] T Holstien, *Ann. Phys*. **8** 343 (1959)
[33] M Eshraghi, P Kameli and H *Salamati J. Theoret. Appl. Phys*.**7** 1 (2013)